J|A|C|S
ARTICLES
Published on Web 01/31/2003

Intercalation of Trioxatriangulenium Ion in DNA: Binding, Electron Transfer, X-ray Crystallography, and Electronic Structure

Jóhannes Reynisson[†,‡] Gary B. Schuster,[*,†] Sheldon B. Howerton,[†] Loren Dean Williams,[*,†] Robert N. Barnett,[§] Charles L. Cleveland,[§] Uzi Landman,[*,§] Niels Harrit,[‡] and Jonathan B. Chaires[||]

Contribution from the Schools of Chemistry and Biochemistry and of Physics, Georgia Institute of Technology, Atlanta, Georgia 30332, Nano-science Center, University of Copenhagen, H.C., Ørsted Institute DK-2100, Copenhagen, Denmark, and Department of Biochemistry, University of Mississippi Medical Center, Jackson, Mississippi 39216

Received August 23, 2002; E-mail: gary.schuster@cos.gatech.edu

Abstract: Trioxatriangulenium ion ($TOTA^+$) is a flat, somewhat hydrophobic compound that has a low-energy unoccupied molecular orbital. It binds to duplex DNA by intercalation with a preference for G-C base pairs. Irradiation of intercalated $TOTA^+$ causes charge (radical cation) injection that results in strand cleavage (after piperidine treatment) primarily at GG steps. The X-ray crystal structure of $TOTA^+$ intercalated in the hexameric duplex $d[CGATCG]_2$ described here reveals that intercalation of $TOTA^+$ results in an unusually large extension of the helical rise of the DNA and that the orientation of $TOTA^+$ is sensitive to hydrogen-bonding interactions with backbone atoms of the DNA. Electronic structure calculations reveal no meaningful charge transfer from DNA to $TOTA^+$ because the lowest unoccupied molecular orbital of $TOTA^+$, $(LUMO)_T$, falls in the gap between the highest occupied molecular orbital, $(HOMO)_D$, and the $(LUMO)_D$ of the DNA bases. These calculations reveal the importance of backbone, water, and counterion interactions, which shift the energy levels of the bases and the intercalated $TOTA^+$ orbitals significantly. The calculations also show that the inserted $TOTA^+$ strongly polarizes the intercalation cavity where a sheet of excess electron density surrounds the $TOTA^+$.

Introduction

Interest in understanding the association of small molecules with duplex DNA is driven by recognition that the precise function of numerous synthetic and natural products that affect DNA chemically or structurally is determined by the mode of binding.[1,2] Intercalation and groove binding are the two most common forms that this association takes. Groove binding is typically observed for arc-shaped, nonplanar compounds that have functional groups able to associate with the hydrogen-bond donors and acceptors found in the major and minor grooves. Binding by intercalation is characteristic of planar, hydrophobic compounds that effectively fill the space produced between base pairs formed when the helix is locally elongated and partially unwound. Intercalated compounds typically interact with adjacent base pairs primarily through van der Waal forces and electrostatic stabilization. Consequently, it appears that polarizable compounds intercalate preferentially at sites containing G-C base pairs since their dipole moment is greater than that of their A-T counterparts.[3]

Extensive investigation of the electronic interaction of compounds intercalated in DNA follows from the important biological and medical roles played by intercalators. Additional interest in investigation of intercalation and stacking was stimulated by the report of accelerated electron transfer between metal complexes mediated by coupling of donor and acceptor states of these compounds with electronic states of the DNA bases.[4] The decisive role of electronic coupling is highlighted by the claimed contrasting behavior of (i) metallointercalators, which elicit the "wirelike" behavior of DNA,[5] (ii) intercalated, tethered ethidium, which must reorient to enable wirelike behavior,[6] and (iii) electron transfer between modified nucleic acid bases, which reveals the invalidity of wirelike behavior.[7]

It seemed that $TOTA^+$ is an ideal compound for examination of the structural, electronic, and chemical effects of an intercalator having a relatively low-energy unfilled orbital. Trioxatriangulenium carbocation ($TOTA^+$, Figure 1)[8] is a stable, planar[9] compound with a relatively low-energy LUMO.[10,11]

[†] School of Chemistry and Biochemistry, Georgia Institute of Technology.
[‡] University of Copenhagen.
[§] School of Physics, Georgia Institute of Technology.
[||] University of Mississippi Medical Center.

(1) Wilson, D. W. *Comprehensive Natural Products Chemistry*; Elsevier Science: New York, 1999; Vol. 7.
(2) Suh, D.; Chaires, J. B. *Bioorg. Med. Chem.* **1995**, *3*, 732−728.
(3) Müller, W.; Crothers, D. M. *Eur. J. Biochem.* **1975**, *54*.
(4) Purugganan, M. D.; Kumar, C. V.; Turro, N. J.; Barton, J. K. *Science* **1988**, *241*, 1645−1649.
(5) Murphy, C. J.; Arkin, M. R.; Jenkins, Y.; Ghatlia, N. D.; Bossman, S. H.; Turro, N. J.; Barton, J. K. *Science* **1993**, *262*, 1025−1029.
(6) Wan, C.; Fiebig, T.; Kelly, S. O.; Treadway, C. R.; Barton, J. K.; Zewail, A. H. *Proc. Natl. Acad. Sci. U.S.A.* **1999**, *96*, 6014−6019.
(7) Wan, C. Z.; Fiebig, T.; Schiemann, O.; Barton, J. K.; Zewail, A. H. *Proc. Natl. Acad. Sci. U.S.A.* **2000**, *97*, 14052−14055.
(8) Martin, J. C.; Smith, R. G. *J. Am. Chem. Soc.* **1964**, *86*, 2252−2256.

10.1021/ja0211196 CCC: $25.00

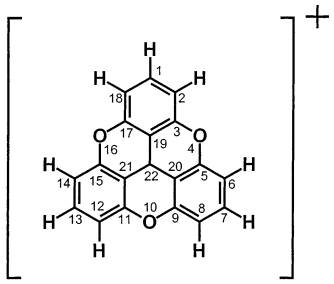

Figure 1. Chemical structure of $TOTA^+$; the numbers are used to identify atomic interactions revealed in the X-ray crystal structure.

Optical excitation of $TOTA^+$ with visible light in aqueous solution forms excited states capable of the one-electron oxidation of guanosine or adenosine.[12]

We report here an investigation of the binding of $TOTA^+$ to DNA oligomers in solution and the photophysical and photochemical reactions of bound $TOTA^+$. Irradiation of bound $TOTA^+$ results in damage at GG steps that is revealed as strand cleavage following treatment with piperidine. This cleavage indicates that light-induced electron transfer from the DNA to the $TOTA^+$ has occurred. We obtained a high-resolution X-ray diffraction of $TOTA^+$ intercalated in the self-complementary hexameric DNA duplex $[d(CGATCG)]_2$. The structure of the DNA·$TOTA^+$ complex allows us to (i) confirm that $TOTA^+$ is an intercalator, (ii) assess the interactions that govern binding orientation and sequence selectivity, (iii) determine the structural consequences to DNA of intercalation of a carbocationic compound that localizes charge near the center of the base pair stack, and (iv) test and extend previous hypotheses on relationships between intercalator structure and DNA distortion.[13]

We also report the results of first-principles quantum mechanical calculations on $TOTA^+$ intercalated in DNA that assess the nature of electronic interactions with adjacent groups of the DNA. To explore the electronic structure and binding characteristics of $TOTA^+$, we performed a series of calculations with the coordinates of the atoms of the DNA·$TOTA^+$ complex taken from the X-ray structure. The calculations were carried out in two stages: (i) we prepared optimized configurations of the intercalation system (including counterions and a hydration shell), using classical molecular dynamics (MD) simulations with the crystallographically determined atomic positions as part of the input; and (ii) we employed quantum mechanical calculations for evaluation of the electronic energy level spectrum of the intercalated DNA molecule, using configurations determined by the MD simulations, for investigation of the bonding mechanism of the intercalated $TOTA^+$ cation to the DNA. These calculations reveal that, despite its low-lying unoccupied orbital, the interactions of $TOTA^+$ with DNA are controlled primarily by hydrophobic, hydrogen-bonding, and electrostatic interactions. There is no significant charge transfer from the DNA to $TOTA^+$ in the ground state.

Materials and Methods

4,8,12-Trioxa-4,8,12,12c-tetrahydrodibenzo[*cd*,*mn*]pyrenylium carbocation ($TOTA^+$) tetrafluoroborate was synthesized according to the procedure published by Martin and Smith.[8]

Determination of the Binding Constant. A sodium phosphate buffer (10 mM) solution of $TOTA^+$ (pH = 7.0, 25 μM in a 1.0 cm cuvette) was titrated with a concentrated calf thymus DNA (CT-DNA) solution. The absorbance of the solution at 330 nm was measured initially and after each addition of CT-DNA. The change in absorbance and the extinction coefficients for $TOTA^+$ in buffer and CT-DNA were used to calculate α, the fraction of DNA-bound $TOTA^+$.[14]

Fluorescence Quenching. Solutions of 25 μM $TOTA^+$ and CT-DNA were prepared in phosphate buffer solution (pH = 7.0) and transferred to a standard 1 cm optical quartz cell. The emission spectrum from 475 to 650 nm was obtained at room temperature on a Spex 1681 Fluorolog emission spectrometer in the normal 90° configuration with excitation at 450 nm.

Solution Viscosity Measurements. Viscosity experiments used a Cannon−Ubbelohbe semimicro dilution viscometer immersed in a thermostated water bath maintained at 33.3 ± 0.02 °C. Small volumes of a concentrated $TOTA^+$ stock solution (5×10^{-4} M) were added to sonicated CT-DNA samples (average 800 base pairs long, 2.4×10^{-4} M in base pairs) in the viscometer. These solutions were mixed by bubbling them with air. The $TOTA^+$ and DNA solutions were buffered with piperazine-*N*,*N*′-bis(2-ethanesulfonic acid) at pH 7.0. Relative viscosities for DNA in either the presence or absence of $TOTA^+$ were calculated from the relation $\eta = (t - t_0)/t_0$, where t is the observed flow time of the DNA-containing solution and t_0 is the flow time of the buffer alone. Viscosity data were plotted as $(\eta/\eta_0)^{1/3}$ versus the binding ratio r, according to the theory of Cohen and Eisenberg.[15]

Induced Circular Dichroic (CD) Spectroscopy. CD spectra of $TOTA^+$ (30 μM in 10 mM sodium phosphate, pH 7) and sonicated CT-DNA (40 μM, base pairs) were recorded on a Jasco J-270 spectrometer in a 10 cm path length cylindrical quartz cell from 200 to 550 nm.

Melting Temperatures (T_m). Melting curves were obtained for $TOTA^+$-containing phosphate buffer solutions of two complimentary 12-mer oligonucleotides d(5′-AAA GGT AAC GCG-3′) and d(5′-CGC GTT ACC TTT-3′), 5 μM in each strand, by monitoring the absorbance at 260 nm on Cary 1E UV−visible spectrophotometer as the temperature was ramped from 20 to 90 °C at the rate of 0.5 °C/min. Melting curves obtained from heating and cooling ramps are essentially identical.

Competition Dialysis. Multiple disposable dialysis units (Spectrum Laboratories, Inc.), each containing 0.5 mL of a 75 μM solution of the DNA sample listed in Table 1, were placed in a beaker containing 200 mL of a 1 μM $TOTA^+$ solution. The system was allowed to equilibrate for 24 h with continuous stirring. After equilibrium was reached, the absorbance of $TOTA^+$ bound to the DNA was measured by extraction into an SDS solution. Since all of the DNA samples are in equilibrium with the same $TOTA^+$ concentration, the amount of bound ligand is directly proportional to the association constant for binding of $TOTA^+$.[16]

Cleavage Analysis. The 12-mer duplex d(5′-AAA GGT AAC GCG-3′) was radiolabeled at the 5′-terminus by use of (γ-^{32}P)ATP and bacterial T4 polynucleotide kinase[17] and purified by 20% PAGE. Samples for irradiation were prepared by hybridizing a mixture of cold and radiolabeled oligonucleotide (5 μM) with 5 μM the complementary strand and 10 μM $TOTA^+$ in a phosphate buffer solution. The samples were irradiated in microcentrifuge tubes in a Rayonet photoreactor containing eight 350 nm lamps. After irradiation, the samples were precipitated with ethanol, dried, and then treated with piperidine (1

(9) Krebs, F. C.; Laursen, B. W.; Johannsen, I.; Faldt, A.; Bechgaard, K.; Jacobsen, C. S.; Thorup, N.; Boubekeur, K. *Acta Crystallogr. B.* **1998**, *55*, 410−423.
(10) Němcová, I.; Němcec, I. *J. Electroanal. Chem.* **1971**, *30*, 506−510.
(11) Reynisson, J.; Balakrishnan, G.; Wilbrandt, R.; Harrit, N. *J. Mol. Struct.* **2000**, *520*, 63−73.
(12) Dileesh, S.; Gopidas, K. R. *Chem. Phys. Lett.* **2000**, *330*, 397−402.
(13) Williams, L. D.; Egli, M.; Gao, Q.; Rich, A. In *DNA Intercalation: Helix Unwinding and Neighbor Exclusion*; Sarma, R. H., Sarma, M. H., Eds.; Adenine Press: Albany, NY, 1992; pp 107−125.
(14) Peacock, A. R.; Skerrett, J. N. *Faraday Soc. Trans.* **1956**, *52*, 261−279.
(15) Cohen, G.; Eisenberg, H. *Biopolymers* **1969**, 45−55.
(16) Ren, J.; Chaires, J. B. *Biochemistry* **1999**, *38*, 16067−16075.
(17) Sambrook, J.; Fritsch, E. F.; Maniatis, T. *Molecular Cloning. A Laboratory Manual*, 2nd ed.; Cold Spring Harbor Laboratory Press: Cold Spring Harbor, NY, 1989.

Table 1. Nucleic Acid Conformations and Samples Used in Competition Dialysis Experiments

conformation	DNA/oligonucleotide	λ^a (nm)	ϵ^b (M^{-1} cm^{-1})	monomeric unit
single-strand purine	poly(dA)	257	8600	nucleotide
single-strand pyrimidine	poly(dT)	264	8520	nucleotide
duplex DNA	*C. perfringens* (31% GC)	260	12 476	base pair
	calf thymus (42% GC)	260	12 824	base pair
	M. lysodeikticus (72% GC)	260	13 846	base pair
	poly(dA)·poly(dT)	260	12 000	base pair
	$[poly(dA\text{-}dT)]_2$	262	13 200	base pair
	$[poly(dG\text{-}dC)]_2$	254	16 800	base pair
DNA-RNA hybrid	poly(rA)·poly(dT)	260	12 460	base pair
duplex RNA	poly(rA)·poly(rU)	260	14 280	base pair
Z DNA[c]	brominated $[poly(dG\text{-}dC)]_2$	254	16 060	base pair
triplex DNA	poly(dA)·$poly(dT)_2$	260	17 200	base triplet
tetraplex DNA 1	$(5'T_2G_{20}T_2)_4$	260	39 267	base tetrad

[a] λ is the wavelength of maximum absorbance. [b] ϵ is the molar extinction coefficient at λ, expressed in terms of the monomeric unit. [c] Prepared according to ref 60.

M) at 90 °C for 15 min. After evaporation of the piperidine, the samples (150 cpm) were separated by electrophoresis on 20% denaturing 19:1 acrylamide−bis(acrylamide) gel containing 7 M urea. Gels were dried and the cleavage was visualized by autoradiography.

Crystallization and Data Collection. Crystals were grown from sitting drops that initially contained 1.6 mM of the ammonium salt of reverse-phase purified d(5′-CGATCG-3′) (Midland Certified Reagent Co., Midland, TX), 18 mM sodium cacodylate (pH 6.5), 22 mM magnesium chloride, 2.7% 2-methyl-2,4-pentanediol (MPD), 0.6 mM spermine tetrachloride, and 1.7 mM $TOTA^+$. The crystallization solution was equilibrated against a reservoir containing 35% MPD at 22 °C. Many dark-red, hexagonal-shaped crystals appeared within 2 weeks. Crystals frozen at 93 K failed to give useful diffraction data despite a variety of attempts to protect the crystals with cryoprotectants. Therefore, data were collected at 295 K. A crystal of 0.2 × 0.2 × 0.2 mm mounted in a 0.3 mm glass capillary diffracted to around 1.6 Å at 295 K. Diffraction data (240°) were collected with 1.54 Å Cu Kα radiation from the in-house Rigaku/MSC rotating anode generator with Osmic blue confocal mirrors and an R-axis IV** image plate detector. A total of 23 527 reflections to 1.55 Å resolution were reduced to a unique data set containing 3168 unique reflections by use of the dtprocess software in the program CrystalClear1.3.0 (R_{merge} = 0.061, 98.1% complete). The space group was determined to be $P6_{5(1)}$ with unit cell dimensions $a = b$ =25.07, c = 82.1, $\alpha = \beta = 90°$, $\gamma = 120°$. Data collection and refinement statistics are presented in the Supporting Information.

Structure Determination and Refinement. The molecular replacement program EPMR[18] was used for phase solution. The starting coordinates for a search model were built from the structure of the hexameric duplex $[d(CGTACG)]_2$ bound to the bisintercalator D232.[19] The D232 molecule was replaced with two $TOTA^+$ molecules, docked at the dCG intercalation steps. The DNA sequence of the search model was known to differ from that of the DNA·$TOTA^+$ complex at the center of the complex. The incorrect sequence was maintained throughout the search so that the molecular replacement solution could be cross-validated by the discrepancy of the model with the electron density maps. A correct solution would show evidence for incorrectly placed and missing atoms of the central base pairs. A solution with an initial correlation coefficient of 59.8 and *R*-factor of 58.6 was refined with the program CNS,[20] using the DNA parameters of Berman and co-workers.[21−23] The parameters for $TOTA^+$ were adapted from the small molecule crystal structure.[9] Planarity of the $TOTA^+$ molecule was restrained. The correctness of the solution was confirmed by cross-validation; the electron density in the center of the complex clearly indicated that the sequence of the search model was incorrect. The sequence of the model was corrected and the two $TOTA^+$ molecules were manually rotated to improve the fit into electron density. The simulated-annealing routine in CNS was performed to help remove bias from the manipulated model. A magnesium ion was added to the model, where it was clearly indicated in the Fourier electron density by its octahedral geometry and characteristic water−magnesium distances. Water molecules were added iteratively to peaks of corresponding sum and difference density followed by refinement and phase recalculation. After the model was completed, the *R*-free was dropped and all data were used to refine the final model. Annealed omit maps were calculated from a model excluding the two $TOTA^+$ molecules. All atoms of both DNA strands and both $TOTA^+$ molecules fit cleanly into the $2F_o - F_c$ and $F_o - F_c$ omit electron density. The geometry of the refined complexes was characterized with the program Curves.[24]

MD Simulations. The classical MD simulations employed the Amber 6 program suite[25] with the AMBER/96 force field [26] (supplemented by partial charges determined by us for $TOTA^+$; see the Supporting Information). In these simulations, the computational cell contained the $[d(CGATCG)]_2$ duplex (including the sugar−phosphate backbone), with $TOTA^+$ intercalated between the two CG steps (i.e., $[d(C/TOTA^+/GATC/TOTA^+/G)]_2$). The atoms of the DNA bases, the backbone, and the $TOTA^+$ were kept (except for the hydrogen atoms) in their crystallographically determined positions. In addition, the computational cell contained eight Na^+ ions and 1610 water molecules, which, together with the DNA hydrogen atoms, were treated dynamically; in constant pressure MD simulations of the system at atmospheric pressure and a temperature of 300 K (STP conditions), the average dimensions of the Cartesian calculational cell were 36.4 Å × 35.7 Å × 41.5 Å, with the larger dimension in the direction of the DNA helix axis. In the MD simulations the equations of motion were integrated by use of the Verlet algorithm with a time step of 1 fs.

Quantum Calculations. First-principles quantum mechanical calculations were performed by the Born−Oppenheimer (BO) local spin

(18) Kissinger, C.; Gehlhaar, D.; Fogel, D. *Acta Crystallogr. Sect. D: Biol. Crystallogr.* **1999**, *55*, 484−491.
(19) Shui, X.; Peek, M. E.; Lipscomb, L. A.; Gao, Q.; Ogata, C.; Roques, B. P.; Garbay-Jaureguiberry, C.; Williams, L. D. *Curr. Med. Chem.* **2000**, *7*, 59−71.
(20) Brunger, A. T.; Adams, P. D.; Clore, G. M.; DeLano, W. L.; Gros, P.; Grosse-Kunstleve, R. W.; Jiang, J. S.; Kuszewski, J.; Nilges, M.; Pannu, N. S.; Read, R. J.; Rice, L. M.; Simonson, T.; Warren, G. L. *Acta Crystallogr. Sect. D: Biol. Crystallogr.* **1998**, *54*, 905−921.
(21) Clowney, L.; Jain, S. C.; Srinivasan, A. R.; Westbrook, J.; Olson, W. K.; Berman, H. M. *J. Am. Chem. Soc.* **1996**, *118*, 509−518.
(22) Parkinson, G.; Vojtechovsky, J.; Clowney, L.; Brunger, A. T.; Berman, H. M. *Acta Crystallogr. Sect. D: Biol. Crystallogr.* **1996**, *52*, 57−64.
(23) Gelbin, A.; Schneider, B.; Clowney, L.; Hsieh, S.-H.; Olson, W. K.; Berman, H. M. *J. Am. Chem. Soc.* **1996**, *118*, 519−529.
(24) Stofer, E.; Lavery, R. *Biopolymers* **1994**, *34*, 337−346.
(25) Case, D. A.; Perlman, D. A.; Caldwell, J. W.; Cheatham, T. E., III; Ross, W. S.; Simmerling, C. L.; Darden, T. A.; Merz, K. M.; Stanton, R. V.; Cheng, A. L.; Vincent, J. J.; Crowley, M.; Tsui, V.; Radmer, R. J.; Duan, Y.; Pitera, J.; Massova, I.; Seibel, G. L.; Singh, U. C.; Weiner, P. K.; Kollman, P. A. *Amber 6*: University of California, San Francisco, 1999.
(26) Kollman, P. A.; Dixon, R.; Cornell, W.; Fox, T.; Chipot, C.; Pohorille, A. *Computer Simulations of Biomolecular Systems*; Elsevier: Amsterdam, 1997; Vol. 3.

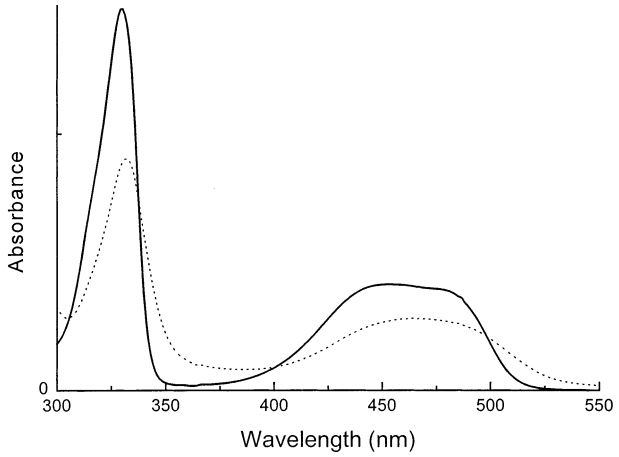

Figure 2. UV−Visible absorption spectra for $TOTA^+$ in buffer solution (solid line) and in the presence of CT-DNA (dashed line).

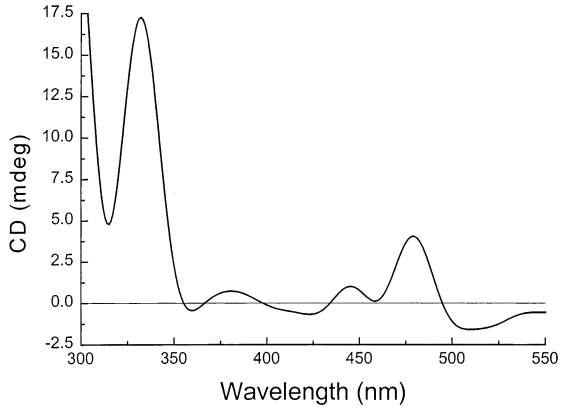

Figure 3. Induced circular dichroic (CD) spectrum of $TOTA^+$ (30 μM in 10 mM sodium phosphate, pH 7) and sonicated CT-DNA (40 μM, base pairs) recorded in a 10 cm path length cylindrical quartz cell.

density (LSD) molecular dynamics (MD) method [BO-LSD-MD],[27] with gradient corrections (generalized gradient approximation, GGA) for the exchange-correlation functional.[28] The Kohn−Sham equations were solved in conjunction with norm-conserving nonlocal pseudopotentals for the valence electrons[29] and a plane-wave basis (i.e., no atom-centered basis functions were used) with a high kinetic energy cutoff of 845 eV; a calculation for the three-base-pair duplex, an intercalated $TOTA^+$, 64 H_2O molecules, and three Na atoms involves 414 ions and 1248 valence electrons. The algorithm for solving the density-functional Kohn−Sham equations uses a Fermi distribution function for the electrons, which is a very effective way of dealing with degenerate or near-degenerate energy levels.[27] The Fermi temperature used is rather low, i.e., 0.01 eV/k_B, which ensures that the Fermi function is operative only on the nearly degenerate levels at the top of the energy level spectrum and not anywhere else (where the spectral gaps are larger). The BO-LSD-MD method is particularly suitable for calculations of charged systems or systems where higher multipole moments may develop, since no periodic replication of the ions is imposed; that is, no supercells are employed.[27] Earlier simulation of hydrated DNA sequences also used the BO-LSD-MD method.[30]

Results and Discussion

(I) Binding and Light-Induced Reactions of $TOTA^+$ with DNA Oligomers in Solution: (1) Association of $TOTA^+$ with DNA. The association of a small molecule with DNA often causes measurable changes to its electronic absorption spectrum that can indicate the mode and strength of binding.[31] We examined the absorption and fluorescence spectra of $TOTA^+$ in the presence of CT-DNA. The three lowest energy absorption bands for $TOTA^+$ in aqueous buffer solution exhibit a pronounced hypochromic effect as well as a bathochromic shift (540−830 cm^{-1}) when CT-DNA is added to the mixture; see Figure 2. The bathochromic effect is most pronounced for the lowest energy absorption band (λ_{max} = 480 nm), and the hypochromicity is greatest for the higher energy transition (λ_{max} = 330 nm).

The equilibrium binding constant for $TOTA^+$ to DNA in 10 mM sodium phosphate buffer solution at pH = 7 was estimated by monitoring the change of its absorption spectrum upon incremental addition of known amounts of CT-DNA. The absorbance of the band with λ_{max} = 330 nm decreased and shifted to lower energy (red) after each addition. Scatchard analysis[32] of these data yields a linear fit, consistent with a single binding mode of $TOTA^+$ to DNA. The estimated binding constant is $(4.1 \pm 0.3) \times 10^4\ M^{-1}$, and the extinction coefficient of the $TOTA^+$·DNA complex is estimated to be 12 200 M^{-1} cm^{-1} at 336 nm. It is difficult to measure the extinction coefficients for the two other transitions of $TOTA^+$, which are in the visible range, due to their overlap.

The circular dichroic (CD) spectrum of $TOTA^+$ bound to DNA provided additional information about the nature of this complex. Binding of an achiral molecule within a chiral environment, such as DNA, can lead to induced optical activity of the bound species.[33] This effect has been observed for a variety of DNA intercalators.[34] Since free $TOTA^+$ is achiral, it has no CD spectrum; however, it exhibits induced CD bands upon binding to CT-DNA as is shown in Figure 3. These bands are relatively weak, which suggests that binding of $TOTA^+$ occurs by intercalation.[35,36]

The electronic interaction of $TOTA^+$ bound to DNA can be assessed by fluorescence spectroscopy. The fluorescence of $TOTA^+$ is quenched by the four individual DNA nucleosides. The Stern−Volmer plots are linear and reveal apparent quenching constants (k_q) of $1.5 \times 10^{10}\ M^{-1}\ s^{-1}$ for 2′-deoxyguanosine and 2′-deoxyadenosine, which is consistent with values reported previously.[12] The fluorescence quenching of $TOTA^+$ by the pyrimidines 2′-deoxycytidine and thymidine is somewhat slower than for the purines with apparent $k_q = 5 \times 10^9\ M^{-1}\ s^{-1}$. These results are not unexpected since, according to the Rehm−Weller equation,[37] the excited singlet state of $TOTA^+$ is a sufficiently strong oxidant to initiate an electron-transfer reaction at the diffusion-limited rate to form the TOTA radical and a purine radical cation.

The effect of CT-DNA on the fluorescence of $TOTA^+$ was examined to assess the effect of binding on the electron-transfer reaction; see Figure 4. As expected, addition of CT-DNA to a $TOTA^+$ solution results in efficient fluorescence quenching.

(27) Barnett, R. N.; Landman, U. *Phys. Rev. B* **1993**, *48*, 2081.
(28) Perdew, P. P. *Phys. Rev. Lett.* **1996**, *77*, 3865.
(29) Troullier, N.; Martins, J. J. *Phys. Rev. B.* **1991**, *43*, 1993.
(30) Barnett, R. N.; Cleveland, C. L.; Joy, A.; Landman, U.; Schuster, G. B. *Science* **2001**, *294*, 567−571.
(31) Bloomfield, V. A.; Crothers, D. M.; Tinoco, I., Jr. *Nucleic Acids: Structure, Properties, and Function*; University Science Books: Sausalito, CA, 1999.
(32) Scatchard, G. *Ann. N.Y. Acad. Sci.* **1949**, *51*, 660−672.
(33) Nordén, B.; Tjerneld, F. *Biopolymers* **1982**, *21*, 1713−1734.
(34) Kubista, M.; Åakerman, B.; Norden, B. *J. Phys. Chem.* **1988**, *92*, 2352−2356.
(35) Lyng, R.; Rodger, A.; Norden, B. *Biopolymers* **1991**, *31*, 1709−1720.
(36) Lyng, R.; Rodger, A.; Norden, B. *Biopolymers* **1992**, *32*, 1201−1214.
(37) Rehm, D.; Weller, A. *Isr. J. Chem.* **1970**, *8*, 259−271.

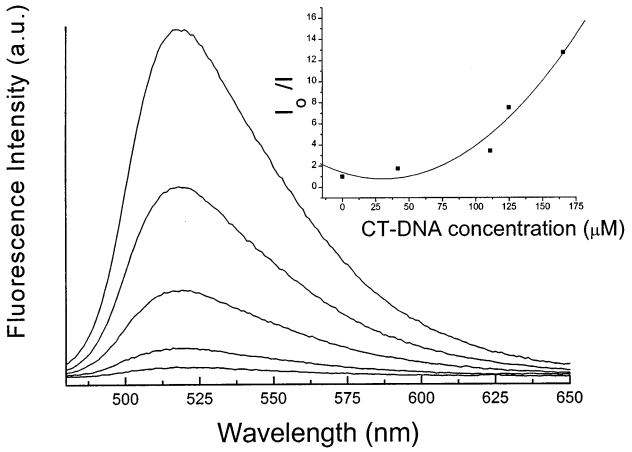

Figure 4. Fluorescence spectra and quenching of $TOTA^+$ (25 μM) by CT-DNA in a phosphate buffer solution (pH = 7.0) at room temperature with excitation at 450 nm. The Stern−Volmer plot is shown as an inset.

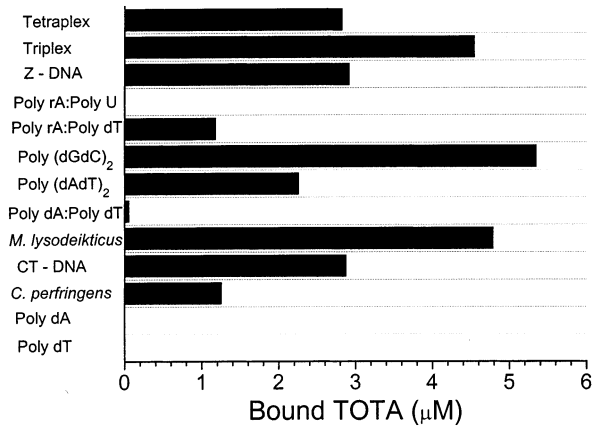

Figure 5. Results from competition binding studies by dialysis after equilibration for 24 h, showing preferential binding to $[poly(dGC)]_2$ and triplex DNA.

Stern−Volmer analysis revealed an upward curving plot, which indicates that dynamic and static quenching processes are active.[38] Irradiation of $TOTA^+$ bound to DNA is expected to result in the rapid injection of a radical cation into the duplex with concomitant formation of the TOTA radical.

The selectivity of $TOTA^+$ binding to various DNA and oligonucleotide structures was further assessed by means of a competition equilibrium dialysis method.[39] The amount of $TOTA^+$ bound at equilibrium in individual buffer solutions containing the nucleic acid oligomers listed in Figure 5 was determined by extraction into a detergent solution and measurement of its optical absorbance. Since all of the DNA samples are in equilibrium with the same concentration of $TOTA^+$, the amount of bound ligand is directly proportional to the association constant for binding of $TOTA^+$.

From the results shown in Figure 5, it is clear that $TOTA^+$ shows a strong inclination for binding to duplex DNA, and is sequence-selective with a preference for C-G base pairs. Interestingly, $TOTA^+$ also shows strong binding to triplex DNA. The apparent affinity of $TOTA^+$ for left-handed Z-DNA probably results from an allosteric conversion to a right-handed form. $TOTA^+$ clearly does not bind significantly to single-stranded DNA or to RNA. These findings are consistent with the binding of $TOTA^+$ to duplex DNA by intercalation.

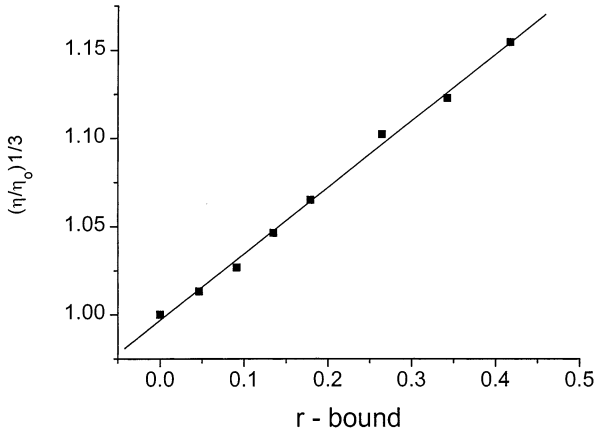

Figure 6. Effect of addition of $TOTA^+$ on the viscosity of solutions buffered with piperazine-*N*,*N*′-bis(2-ethanesulfonic acid) at pH = 7.0 and containing CT-DNA (averaging 800 base pairs, 2.4×10^{-4} M in base pairs). The temperature was maintained at 33.3 ± 0.02 °C. The viscosity data were plotted as $(\eta/\eta_0)^{1/3}$ versus the binding ratio, *r*, according to the theory of Cohen and Eisenberg.[15]

The data of Figure 5 can be used to quantitatively evaluate binding. First, the apparent binding constant may be calculated from the equation $K_{app} = C_b/[C_f - (C_T - C_b)]$, where C_b is the amount of $TOTA^+$ bound plotted in Figure 5, C_f is the free $TOTA^+$ concentration (fixed at 1 μM), and C_T is the total nucleic acid concentration (fixed at 75 μM). For binding to CT-DNA, the data shown in Figure 5 yield $K_{app} = 4.0 \times 10^4\ M^{-1}$, a value in excellent agreement with the binding constant determined by spectrophotometric titrations as described above. Second, the data for *Clostridium perfringens* and *M. lysodeikticus* DNA samples may be used to calculate the ratio $\alpha = C_b(M.\ lysodeikticus)/C_b(C.\ perfringens) = 3.8$. The magnitude of α provides an indication of the nature of the preferred DNA binding site.[40] The value 3.8 corresponds most closely to the value of α predicted for a preferred binding site composed of adjacent GC base pairs. Photocleavage data, presented later, is fully consistent with such a preferred binding site.

Solution viscosity measurements provide a means to distinguish intercalation from groove binding. In fact, hydrodynamic determination of length changes is among the most stringent tests of the binding mode of ligands to DNA.[41−43] If a compound binds in a DNA groove, without intercalating, only modest changes in viscosity are generally observed, since this has little effect on the effective length of the polymer. Intercalation, on the other hand, proceeds by unwinding the double helix to accommodate a compound that becomes inserted and stacked between the base pairs. This process results in an effective increase in the DNA contour length. Figure 6 shows the results obtained from viscosity measurements of sonicated CT-DNA (on average 800 base pairs long, 2.4×10^{-4} M in base pairs) with increasing amounts of bound $TOTA^+$. Evidently, $TOTA^+$ increases the length of DNA, resulting in an increased viscosity, which suggests that it binds to DNA by intercalation. However,

(38) Lakowicz, J. *Principles of Fluorescence Spectroscopy*; Plenum Press: New York, 1983.
(39) Ren, J. S.; Chaires, J. B. *Methods Enzymol.* **2001**, *340*, 99−108.
(40) Chaires, J. B. *Advances in DNA Sequence Specific Agents*; JAI Press: Greenwich, CT, 1992; Vol. 1.
(41) Bloomfield, V. A.; Crothers, D. M.; Tinoco, I., Jr. *Physical Chemistry of Nucleic Acids*; Harper & Row: New York, 1974.
(42) Dougherty, G.; Pilbrow, J. R. *Int. J. Biochem.* **1984**, *16*, 1179−1192.
(43) Wilson, W. D.; Jones, R. L. *Intercalation Chemistry*; Academic Press: New York, 1982.

Figure 7. PAGE (after treatment with piperidine) showing the effects of irradiation of a phosphate buffer solution containing 5 μM duplex (5′-AAA GGT AAC GCG-3′), labeled at the 5′-terminus with ^{32}P, and 10 μM TOTA$^+$ at 350 nm for 1 and 2 h (lanes ii and i, respectively). Strand cleavage is observed primarily at the 5′-G of the GG step. No cleavage was observed for unirradiated samples.

the apparent length increase of 1.3 Å per intercalated TOTA$^+$ is somewhat less than is observed for other intercalating agents.[44−46] The length of the DNA samples used in these experiments is longer than the DNA persistence length (≈150 bp), which suggests that the samples will have some flexibility. The lower than expected value for the lengthening could result from changes in the flexibility superimposed on the lengthening.

(2) Cleavage of DNA Photoinduced by TOTA$^+$. The one-electron oxidation of DNA results in the formation of a base radical cation that migrates through the DNA duplex by a hopping mechanism and causes the selective reaction at the 5′-G of GG steps. Reaction at guanine is typically revealed as strand cleavage by treatment of the irradiated sample with hot piperidine. Strand cleavage is detected by gel electrophoresis and autoradiography.[47−50] We examined the light-induced reaction of TOTA$^+$ bound to the duplex oligonucleotide d(5′-AAAGGTAACGCG-3′), which was radiolabeled at the A of its 5′-terminus with ^{32}P.

Association of TOTA$^+$ with the duplex oligonucleotide was confirmed by optical spectroscopy and melting temperature (T_m) experiments. The T_m of a 5 μM solution of the duplex oligomer in 10 mM phosphate buffer at pH = 7.0 increases from 52.8 to 57.3 °C when 5 μM TOTA$^+$ is added.

Solutions containing the radiolabeled duplex oligomer (5 μM) and bound TOTA$^+$ (5 μM; the concentration of free TOTA$^+$ in solution is calculated to be ca. 30 nM) were irradiated at 350 nm for 2 h in a Rayonet photoreactor. After irradiation, the DNA was precipitated, treated with hot piperidine, analyzed by denaturing gel electrophoresis, and visualized by autoradiography. Strand cleavage is observed selectively at the 5′-G of GG step of the oligomer; see Figure 7. No cleavage is observed for unirradiated samples. These results indicate that, when bound to DNA, the excited state of TOTA$^+$ oxidizes the DNA. This reaction is relatively inefficient, as indicated by the long irradiation time required, which is probably a consequence of its origination from a singlet excited state of TOTA$^+$ that generates a singlet radical ion pair that is prone to rapid annihilation by back electron transfer.[49]

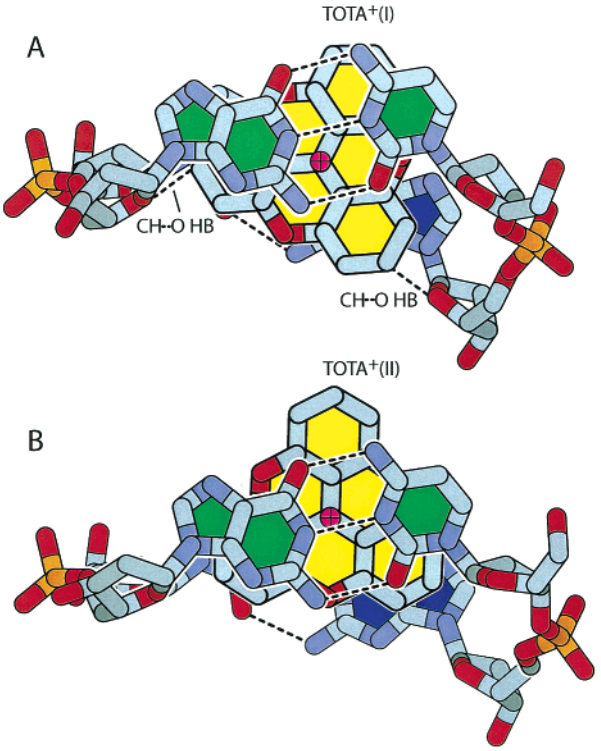

Figure 8. Axial views of the [d(CGATCG)]$_2$·TOTA$^+_2$ X-ray structure. The base pairs are shaded: terminal base pair, green; internal base pair, blue. TOTA$^+$ molecules are shaded yellow. The formal carbocation is indicated by a plus sign. Hydrogen bonds are indicated by dashed lines. C−H···O hydrogen bonds are labeled. (A) TOTA$^+$(I); (B) TOTA$^+$(II).

(II) Three-Dimensional Structure of a [d(CGATCG)]$_2$·TOTA$^+_2$ Complex. The X-ray data reveal a complex composed of the hexameric duplex plus two TOTA$^+$ molecules intercalated at each terminal base pair step. The DNA residues are numbered 5′-C(1)G(2)A(3)T(4)C(5)G(6)-3′ and 5′-C(7)G(8)A(9)T(10)C-(11)G(12)-3′. TOTA$^+$(I) is intercalated between base pairs C(1)-G(12) and G(2)-C(11), and TOTA$^+$(II) is intercalated between base pairs C(5)-G(8) and G(6)-C(7). Each crystallographic asymmetric unit contains two DNA strands and two TOTA$^+$ molecules, and each [d(CGATCG)]$_2$·TOTA$^+_2$ complex contains a noncrystallographic pseudo-2-fold axis between base pairs A(3)-T(10) and T(4)-A(9).

(1) DNA−TOTA$^+$ Interactions. The aromatic faces of the TOTA$^+$ ring systems are engaged in stacking interactions with the adjacent cytosines and guanines. TOTA$^+$(I) is more centrally disposed relative to the major and minor grooves and seems to engage in tighter interactions with the DNA than TOTA$^+$(II); see Figure 8. TOTA$^+$(I) engages in a greater number of contacts (a contact is defined as an interatomic distance < 3.4 Å) with the DNA than TOTA$^+$(II). TOTA$^+$(II) is partially extruded out into the major groove. TOTA$^+$(I) is in contact with nine, and TOTA$^+$(II) is in contact with seven, atoms of the flanking base pairs. These stacking contacts are significantly longer than some of the TOTA$^+$−backbone contacts (see below). The formal

(44) Waring, M. J. *Annu. Rev. Biochem.* **1981**, *50*, 159−192.
(45) Waring, M. J.; Gonzalez, F. A.; Jimenez, A.; Vazques, D. *Nucleic Acids Res.* **1979**, *7*, 217−230.
(46) Baez, A.; Gonzalez, F. A.; Vazquez, D.; Waring, M. J. *Biochem. Pharmacol.* **1983**, *32*, 2089−2094.
(47) Sugiyama, H.; Saito, I. *J. Am. Chem. Soc.* **1996**, *118*, 7063−7068.
(48) Nunez, M.; Hall, D. B.; Barton, J. K. *Chem. Biol.* **1999**, *6*, 85−97.
(49) Schuster, G. B. *Acc. Chem. Res.* **2000**, *33*, 253−260.
(50) Giese, B. *Acc. Chem. Res.* **2000**, *33*, 631−636.

carbocationic center at C22 (Figure 1) of the $TOTA^+$ molecules is centrally disposed relative to the flanking base pairs and falls near to the helical axis. However, neither of the formal carbocations is in contact with DNA atoms. Both are closer to O6 and N1 atoms of guanine residues than to other atoms. The C22 of $TOTA^+$(I) is 3.6 A from both the O6 of G(8) and the N1 of G(6). The C22 of $TOTA^+$(II) is 3.6 Å from both the O6 of G(2) and the N1 of G(12).

The shortest DNA−$TOTA^+$ contacts are not with the flanking bases but with backbone atoms. Indeed, the O4′ atoms that partially compose the wall of the intercalation cavity [G(6) O4′ and G(8) O4′] appear to interact with electron-deficient carbon atoms of $TOTA^+$(I). The C1 of $TOTA^+$(I) is 2.8 Å from the O4′ of G(8), and the C7 is 3.1 Å from the O4′ of G(6). These interactions satisfy established geometric criteria for C−H···O hydrogen bonds,[51] with a C4′−O4′−C1 angle of 126° and a C4′−O4′−C7 angle of 136°. These C−H···O hydrogen bonds appear to contribute to a favorable free energy of interaction with the DNA and anchor the $TOTA^+$ within the intercalation cavity (Figure 8). This hypothesis is supported by the observation that $TOTA^+$(II), which is less firmly fixed in position, forms a single long C−H···O contact with the backbone [3.4 Å, C1 to O4′ of G(12)].

As expected from the greater number of contacts with the DNA, including the C−H···O hydrogen bonds, the position of $TOTA^+$(I) is more highly ordered than that of $TOTA^+$(II). The thermal factors of $TOTA^+$(I) are lower than those of $TOTA^+$-(II), and the electron density maps are more finely detailed.

With the exception of the C−H···O interactions, $TOTA^+$ does not appear to engage in directional contacts with the functional groups on the DNA bases or with solvent molecules. None of the oxygen atoms of either intercalated $TOTA^+$ molecule has the correct geometry relative to the DNA to form hydrogen bonds. The O4 oxygen of $TOTA^+$(I) and the O10 of the symmetry-related $TOTA^+$(II) are separated by 3.27 Å. Both of these ether oxygen atoms are hydrogen-bond acceptors and there is no potential for hydrogen bonding in this interaction.

(2) DNA Conformation. The base-pair translations that accompany intercalation of $TOTA^+$ appear to be measurably greater than those for other intercalators. This translation is quantified by the helical rise per base pair at the C(1)-G(12)/G(2)-C(11) and the C(5)-G(8)/G(6)-C(7) steps. The helical rise is 7.10 Å at the intercalation cavity of $TOTA^+$(II) and 7.37 Å at the cavity of $TOTA^+$(I). By comparison, the average corresponding value observed in 10 high-resolution intercalative complexes in a analogous comparison set obtained from the NDB[52] (Nucleic Acid Database) is 7.03 Å, with a limiting value of 7.08 (see Supporting Information). The helical rise at the G(2)-C(11)/A93)-T(10) step and at the T(4)-A(9)/C(5)-G(8) steps is inordinately large. The average for the comparison set is 3.18 Å, with the most extreme value of 3.49 Å. The corresponding values in the $TOTA^+$ complex are 3.60 for $TOTA^+$(II) and 3.68 Å for $TOTA^+$(I). The unusual helical rise value combine to give the total length of the $TOTA^+$ complex of 24.7 Å, which is significantly greater than the average of the comparison set (23.6 Å) and is greater than the limiting value (23.7 Å).

The minor-groove width of the $[d(CGATCG)]_2$·$TOTA^+_2$ complex in the central region of the complex is approximately 9 Å, considerably wider than the 7.5 Å width of the $[d(CGATCG)_2]$·daunomycin complex (NDB ID DDF018). The $[d(CGATCG)]_2$·$TOTA^+_2$ complex is also bent to a significant extent as compared with DNA/intercalator complexes of similar sequence. When compared with the relatively straight $[d(CGTACG)]_2$·D232 complex, the curvature is quite noticeable. The overall bend angle of the $TOTA^+$ complex is approximately 18°; the complex is bent toward the major groove.

(3) Water/Cation Region. The solvent region surrounding the DNA·$TOTA^+$ complex is not particularly well characterized in this structure because the X-ray data were collected at room temperature. However, the electron density maps clearly reveal a magnesium ion with six coordinating water molecules within the major groove of the DNA·$TOTA^+$ complex. The first-shell water molecules interact with the N7 and O6 positions of G(2) [N7−W2, 2.7 Å; O6−W5, 2.7 Å] and the O4 of T(4) (O4−W3, 2.8 Å). The water molecules of the $Mg(H_2O)_6^{2+}$ are involved in lattice interactions with phosphate groups of a symmetrically related complex. The $Mg(H_2O)_6^{2+}$ is not within contact distance of either $TOTA^+$ molecule. Seventeen additional water molecules were identified in the electron density map. None of these water molecules is within contact distance with any of the oxygen atoms of $TOTA^+$. The minor groove of $[d(CGATCG)]_2$·$TOTA^+_2$ is devoid of water molecules. Entry of water molecules into the minor groove is precluded by symmetry-related DNA·$TOTA^+$ complexes. The packing arrangement is similar to that in the $[d(CGTACG)]_2$·D232 complex. A 6-fold screw axis generates duplexes that repeat in the direction parallel to the long axis of each unit cell. Each duplex is tilted such that there is no continuous helix.

(4) Features of the Structure of the $[d(CGATCG)]_2$·$TOTA^+_2$ Complex. The essential DNA deformation required for intercalation involves translation of the base pairs in opposing directions along the helical axis, to form an intercalative cavity.[53] This base-pair translation disrupts base−base stacking interactions, which are offset at least in part by base−intercalator interactions. The base-pair translations of the $TOTA^+$ complex are greater than those of other intercalators, and the complex appears to be extended at both intercalation steps. The unusual extension is related to unfavorable electronic or electrostatic interactions between $TOTA^+$ and DNA; neither of the formal carbocations of the two $TOTA^+$ molecules is in contact with DNA atoms (<3.6 Å).

DNA deformation can extend along the helical axis into sequences flanking the intercalation site. In the $TOTA^+$ complex, an unusual deformation is observed at the base pair steps adjacent to the intercalation steps [i.e., at the G(2)-C(11)/A93)-T(10) step and at the T(4)-A(9)/C(5)-G(8) step]. The helical rise at these steps is inordinately large. Solution experiments, reported above, show that intercalation of $TOTA^+$ into DNA causes increases in viscosity to a lesser extent than other intercalators do. This may be due to unusual flexibility introduced into the DNA by the $TOTA^+$. The extended helical rise decreases stacking contacts and possibly facilitates DNA bending.

As noted above, the electron density maps clearly reveal a magnesium ion with six coordinating water molecules within

(51) Jeffrey, G. A.; Saenger, W. *Hydrogen Bonding in Biological Structures*; Springer-Verlag: New York, 1991.
(52) Berman, H. M.; Zardecki, C.; Westbrook, J. *Acta Crystallogr. Sect. D: Biol. Crystallogr.* **1998**, *54*, 1095−1104.
(53) Lerman, L. S. *J. Mol. Biol.* **1961**, *3*, 18−30.

the major groove of the DNA·TOTA$^+$ complex. The first-shell water molecules interact with the N7 and O6 positions of G(2) and the O4 of T(4). As proposed previously, divalent cations, usually hydrated, and monovalent cations, usually dehydrated, localize adjacent to B-DNA by favorable interaction with the O6 and N7 groups of guanine within the major groove and with the O2 groups of thymine and the N3 groups adenine within the minor groove.[54−57] The magnesium ion here follows that pattern of interaction and appears to facilitate the observed helical bend toward the major groove. Localized cations, within G-tract major grooves and A-tract minor grooves, are proposed to interact through electrostatic interactions with DNA phosphate groups and facilitate DNA bending and other deformations (electrostatic collapse). However, as with other X-ray derived structures, the electrostatic interactions within the present complex cannot be fully characterized by the final refined model. With a total anionic charge of 10 and a total cationic charge of 4, the structure here does not achieve charge neutrality. Additional cations, either ordered or disordered, are contained within the solvent region. In some cases lattice effects are known to cause DNA bending in crystals.[58] A comparison of the [d(CGATCG)]$_2$·TOTA$^+_2$ complex with a [d(CGTACG)]$_2$·D232 complex suggests that bending of [d(CGATCG)]$_2$·TOTA$^+_2$ does not originate from lattice interactions. These two complexes have nearly equivalent packing arrangements, including the locations of symmetry-related nucleotides across the minor groove, which appear to widen the minor groove. However, the [d(CGTACG)]$_2$·D232 complex is linear.

In summary, these findings show that TOTA$^+$(I) and TOTA$^+$-(II) form crystallographically distinct intercalative complexes that have differing orientations and interactions. TOTA$^+$(I) is centrally disposed relative to the major and minor grooves, engages in tighter interactions with the DNA, and is more firmly fixed in position than TOTA$^+$(II), which is partially extruded out into the major groove. The shortest DNA−TOTA$^+$ contacts are not with the flanking bases but with backbone atoms. Electron-deficient and relatively acidic CH groups of TOTA$^+$-(I) form hydrogen bonds with O4′ oxygen atoms embedded in the walls of the intercalation cavities. These intracavity C−H···O hydrogen bonds appear to confer stability and orientation specificity to TOTA$^+$. TOTA$^+$(I) forms two short C−H···O hydrogen bonds, while TOTA$^+$(II) forms one long C−H···O hydrogen bond. Intracavity hydrogen bonding has not, to our knowledge, been observed previously and may represent a generalizable DNA recognition device. Substitution of the hydrogen-bonding CH groups with appropriately oriented NH or OH groups should substantially increase the affinity.

(III) Electronic Structure Calculations of the [d(CGATCG)]$_2$·TOTA$^+_2$ Complex: (1) Molecular Dynamics to Locate Hydrogen Atoms, Water Molecules, and Counterions. Detailed electronic structure calculations were preceded by a classical molecular dynamics simulation to obtain an optimized configuration of the intercalated TOTA$^+$ in the hydrated hexameric duplex that includes the requisite counterions. The simulation starts from a model of the system with the coordinates of all the atoms of the DNA bases and the intercalated TOTA$^+$ molecules (except the hydrogen atoms) taken from the X-ray data (and held constant throughout the optimization process). This configuration was supplemented by hydrogen atoms and by sodium cations that were added at positions in the vicinity of the backbone phosphate groups to achieve overall electrical neutrality. Finally, the system was embedded in a "water bath" consisting of 1610 water molecules, the computational cell was periodically replicated (through the use of periodic boundary conditions), and the system was equilibrated at 300 K and 1 atm. A configuration was then selected from the equilibrium ensemble, and the periodic boundary conditions were removed. Subsequently, all water molecules whose atoms were distanced by more then 5 Å from any atom of the solute (i.e., DNA oligomer, intercalated TOTA$^+$, and the sodium cations) were removed, leaving a hydration shell of 422 molecules. This step was followed by several simulated annealing cycles, in conjunction with a procedure aimed at contracting the hydration environment to the "minimal" one. In each of these cycles the hydration environment was heated gradually (via velocity scaling) to about 270 K (with the non-hydrogen atoms of the DNA and TOTA$^+$ molecules held fixed), and after evolving dynamically at that temperature (typically for about 20 ps), the system was gradually cooled to 0 K and the structure of the hydration environment (as well as the locations of the hydrogens

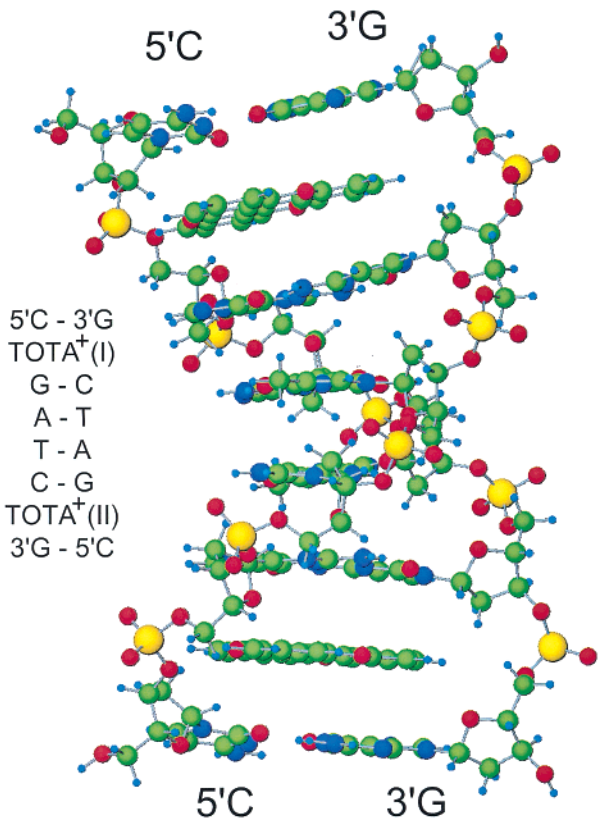

Figure 9. [d(CGATCG)]$_2$·TOTA$_2^+$ complex, with the coordinates of all the atoms taken from the X-ray structure except the hydrogens, whose coordinates were computed as described in the text. The hydrating water molecules and counterions, which were included in the molecular dynamics simulations, are not shown for clarity. The various chemical species are depicted as follows: C in green, N in blue, O in red, and P in yellow; small blue spheres correspond to hydrogen atoms. The order of the nucleotide bases and the TOTA cations is indicated on the left.

(54) Hud, N. V.; Feigon, J. *J. Am. Chem. Soc.* **1997**, *119*, 5756−5757.
(55) Hud, N. V.; Sklenar, V.; Feigon, J. *J. Mol. Biol.* **1999**, *286*, 651−60.
(56) Howerton, S. B.; Sines, C. C.; VanDerveer, D.; Williams, L. D. *Biochemistry* **2001**, *40*, 10023−10031.
(57) Sines, C. C.; McFail-Isom, L.; Howerton, S. B.; VanDerveer, D.; Williams, L. D. *J. Am. Chem. Soc.* **2000**, *122*, 11048−11056.
(58) DiGabriele, A. D.; Sanderson, M. R.; Steitz, T. A. *Proc. Natl. Acad. Sci. U.S.A.* **1989**, *86*, 1816−1820.

of the DNA and the intercalators) was optimized by an energy-gradient minimization method. Subsequently, a histogram of the molecular hydration energies was constructed, and it was employed (together with visual inspection and analysis of the connectivity and coordination of the hydrogen-bond network in the solvation shell) in deciding which water molecules may be discarded, while the more tightly bound ones are maintained. Successive iterations of the above procedure (with each cycle resulting in a smaller number of water molecules retained in the "intimate" hydration environment), culminated in a "minimal hydration shell" (consisting of 120 water molecules) that solvates the intercalated system (including the sodium counterions). The optimized configuration of the intercalated system (with the non-hydrogen atoms of the DNA and the $TOTA^+$ intercalators taken from the crystallographical data) is shown in Figure 9, where the counterions and the hydration shell have been excluded for clarity.

To enhance the feasibility of electronic structure calculations on the intercalated system (see below), we have taken advantage of the self-complementary character of the DNA oligomer used in this study. Accordingly, the hydrated six-base-pair intercalated system described above was split into two halves, with each half containing three base pairs, an intercalated $TOTA^+$(I or II), three sodium counterions, and a hydration shell consisting of the 64 water molecules closest to the selected half. The two "half-configurations" were then further annealed (through a cycle of gradual heating and subsequent gradual cooling), resulting in optimal configurations suitable for the quantum calculations described below; atomic configurations of the two hydrated halves are displayed in Figure 13.

(2) Quantum Mechanical Calculations. Figure 10 shows the electronic energy level schemes (only eigenvalues with energies higher than −12 eV are included), calculated for the following: (i) the "stretched" three-base-pair d(5′-C//GA-3′)-[4Na] duplex segment of the intercalated hexameric duplex but without the inserted $TOTA^+$ (the symbol // represents the expanded interbase distance at the intercalation site, along the axis of the double helix), in which the positions of the DNA atoms were taken from the crystallographic data determined for the intercalated system (except for the hydrogen atoms); (ii) the isolated $TOTA^+$, with crystallographically determined heavy atomic positions; (iii) the unhydrated $TOTA^+$-intercalated neutral three-base-pair duplex d(5′-C/$TOTA^+$/GA-3′)[3Na], with the DNA and $TOTA^+$ coordinates crystallographically determined for the half of the intercalated six-base-pair DNA oligomer that contains $TOTA^+$(I); (iv) same as in column iii but with a hydration shell; and (v) same as in column iv but for the half of the six-base-pair oligomer containing $TOTA^+$(II). Each of the added Na atoms "donates" an electron to the DNA (with the negative charges localizing mostly on the phosphate groups) and thus become the sodium counterions.

Inspection of the eigenvalue schemes of the unhydrated "stretched" three-base-pair DNA duplex segment, d(5′-C//GA-3′)[4Na] [corresponding to the $TOTA^+$(I) site; see Figure 9] and of the isolated $TOTA^+$ (columns i and ii) shows that both the highest occupied molecular orbital $(HOMO)_T$ and the lowest unoccupied one $(LUMO)_T$ of $TOTA^+$ lie well below the $(HOMO)_D$ of the "stretched" DNA segment, where subscripts T and D indicate the orbital's predominant association with the $TOTA^+$ or the DNA, respectively, where such a designation is

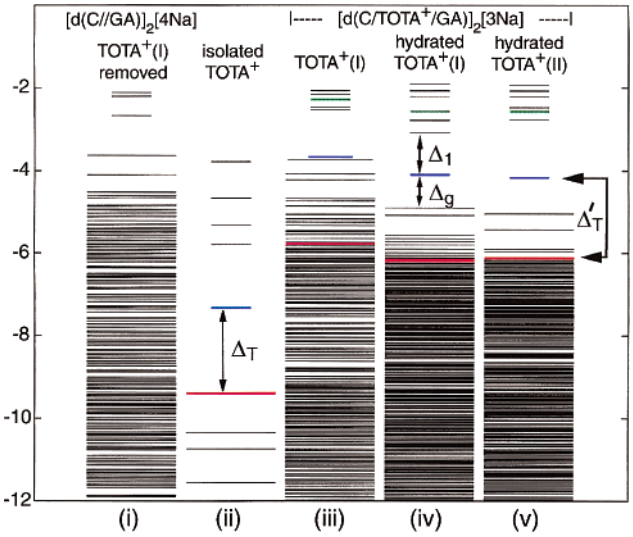

Figure 10. Calculated electronic energy level schemes for various components of the intercalation complex. Only eigenvalues with energies higher than −12 eV are displayed. Long horizontal lines correspond to occupied levels, and short lines denote unoccupied ones. The schemes correspond to the following systems (from left to right): (i) "stretched" 3-bp duplex segment d(5′-C//GA-3′)$_2$[4Na], where // denotes the empty $TOTA^+$(I) site; (ii) isolated $TOTA^+$, with the electronic structure calculated for the crystallographically determined heavy atom positions and with the coordinates of the hydrogens determined through optimization employing the Amber 6 force field supplemented by partial charges that were determined as described in the Supporting Information. Δ_T denotes the energy gap between the $(HOMO)_T$ and $(LUMO)_T$ levels that are colored red and blue, respectively. The unoccupied level above the $(LUMO)_T$, i.e., $(LUMO + 1)_T$, is colored green. The level schemes in columns iii and iv correspond to the 3-bp segment shown in column i but with $TOTA^+$(I) inserted at the CG step. The level scheme in column iii was calculated for the unhydrated system (but including the counterions), and the scheme in column iv was calculated for the hydrated system, illustrating the stabilizing effect due to hydration. The colored levels denote the positions of the corresponding eigenvalues of the isolated $TOTA^+$ (as described for column ii) but after intercalation. In column iv, Δ_g denotes the energy gap between the HOMO and LUMO levels of the complex, and Δ_1 corresponds to the energy separation between the LUMO and (LUMO + 1) levels of the complex. (v) Energy level scheme for the hydrated intercalated complex, calculated for the 3-bp DNA segment associated with $TOTA^+$(II). Δ_T' denotes the energy separation between the level corresponding to the HOMO of the isolated $TOTA^+$ (colored red) and the LUMO of the intercalation complex (colored blue).

meaningful. In the isolated $TOTA^+$, the calculated energy gap between the $(HOMO)_T$ and $(LUMO)_T$ levels is $\Delta_g = 2.08$ eV (to facilitate discussion, we interchangeably refer to Δ_g of the isolated $TOTA^+$ also as Δ_T; see Figure 10). This suggests that charge transfer to the intercalated $TOTA^+$ may occur. In this context we note that the energy levels of the unhydrated native three-base-pair DNA segment (not shown) are higher than those of the corresponding unhydrated "stretched" DNA segment (see column i in Figure 10), reflecting the relative instability of the former that is associated with the lack of hydration.

Comparison of the energy level schemes shown in Figure 10 for the unhydrated (iii) and hydrated (iv) intercalated complexes corresponding to the $TOTA^+$(I) site illustrates the marked effect of hydration on the electronic structure of the intercalated DNA system. For the unhydrated complex (iii), the $(LUMO)_T$ is almost degenerate with the $(HOMO)_D$ (a separation of $\Delta_g = 0.06$ eV), with a gap $\Delta = 1.19$ eV between the $(LUMO)_T$ and the next higher energy unoccupied molecular orbital, which is associated primarily with the DNA. However, as a result of hydration, the entire electronic energy level spectrum of the

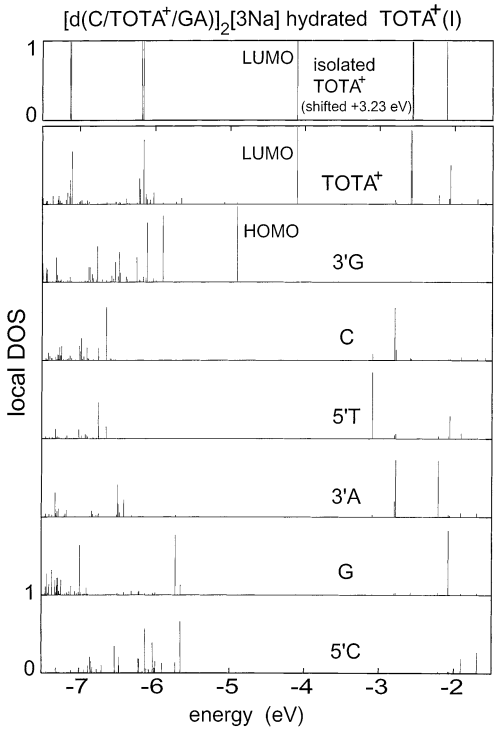

Figure 11. Local densities of states (LDOS) calculated for the isolated $TOTA^+$ (top panel) and for the hydrated $TOTA^+$(I) 3-bp DNA segment. The LDOS of the isolated $TOTA^+$ has been rigidly shifted by 3.23 eV. In each panel we depict the weighted local DOS in the denoted region (see lettered designation in each panel). The height of a vertical bar denotes the weight of the LDOS (corresponding to the energy given on the horizontal axis) in the specified spatial region. A weight of 1 corresponds to full localization of the energy level in a particular region; for example, the HOMO level of the intercalation complex is seen to be fully localized on the 3′G and the LUMO level is fully localized on the inserted $TOTA^+$. Note the correspondence between the (shifted) LDOS of the isolated $TOTA^+$ and that corresponding to the intercalated $TOTA^+$(I).

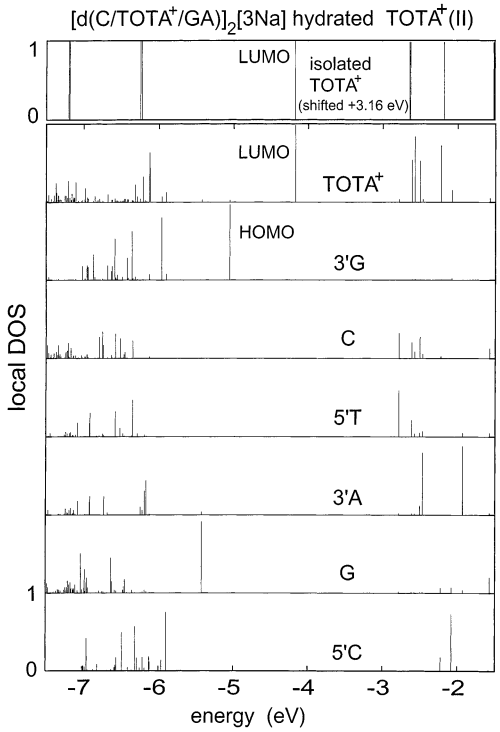

Figure 12. Local densities of states, as in Figure 11, but for the hydrated $TOTA^+$(II) 3-bp duplex DNA segment.

complex shifts to lower energies, and the separation between the $(HOMO)_D$ and $(LUMO)_T$ levels increases significantly ($\Delta_g = 0.81$ eV); in fact, the $(LUMO)_T$ of the hydrated complex (see column iv in Figure 10) appears as a level in the gap between the $(HOMO)_D$ and the second unoccupied level ($\Delta_1 = 1.01$ eV). The energy level spectrum of the hydrated intercalated complex calculated for the three-base-pair DNA segment associated with $TOTA^+$(II), see column v in Figure 10, shows characteristics similar to those discussed above, with certain quantitative differences that reflect the crystallographic nonequivalence of the two: e.g., $\Delta_g = 0.9$ eV and $\Delta_1 = 1.39$ eV.

Further insights into the nature of the intercalation complex are obtained from analysis of the weighted local density of states (LDOS), where for a given energy eigenvalue the (weighted) probability distribution of the corresponding (normalized) wave function (molecular orbital) in different (spatial) regions of the intercalated system is determined through integration of the square of the wave function in the various regions.[59] Plots of the weighted LDOS calculated for the $TOTA^+$(I) and $TOTA^+$-(II) segments are shown in Figures 11 and 12, respectively. In these figures, the electronic energy spectrum of the isolated $TOTA^+$ is uniformly shifted to higher energy so that the $(LUMO)_T$ of the isolated $TOTA^+$ will align with the $(LUMO)_T$ of the intercalated $TOTA^+$ (shifts of 3.23 and 3.16 eV were used in Figures 11 and 12, respectively). Interestingly, we find that for both intercalation sites the $(LUMO)_T$ level of the complex is fully localized (that is, we find an LDOS with a weight of unity) on the inserted $TOTA^+$. Moreover, the $(LUMO)_T$ calculated for the $TOTA^+$(I) and $TOTA^+$(II) segments are essentially identical to the $(LUMO)_T$ of the isolated $TOTA^+$ (see portraits of the orbitals in the top row of Figure 13). These observations, coupled with the finding that the integrated charge in the intercalation region is close to +1, show that intercalation of $TOTA^+$ into the DNA is not accompanied by transfer of charge from the DNA.

Apparent also from Figures 11 and 12 is that for both intercalation sites the $(HOMO)_D$ is localized almost entirely on the 3′-G (see also orbital plots in the second row of Figure 13). The $(HOMO)_T$ and $(HOMO - 1)_T$ states of the isolated $TOTA^+$ are quasidegenerate (see the red-colored eigenvalues in the column marked isolated $TOTA^+$ in Figure 10, the top panel of Figure 11, and the corresponding orbital plots in Figure 13). Analysis of the orbital overlaps between these states and various states near the top of the energy spectrum of the intercalation complex allowed us to identify the eigenfunctions of the complex with maximal overlap to the $(HOMO)_T$ and $(HOMO - 1)_T$ states of the isolated $TOTA^+$. The states of the complex with maximal overlap are colored red in columns iv and v of

(59) A region (for the purpose of calculating the local density-of-states as well as other local properties) is defined as the union of spheres centered on the atoms that belong to that region, for example, the atoms of a nuclear base, of the sugar−phosphate backbone, or of the $TOTA^+$ molecule. The radii of the spheres are taken as 2.1 Å for C, N, O, P, and Na and 0.53 Å for a hydrogen atom. Note that with this definition there is some overlap of regions; in particular, the base regions overlap with the backbone region and to a lesser extent with the water region. There is little overlap between the regions of the different bases (the base-to-base distance along the axis of the helix is 3.4 Å) or between a base region and the $TOTA^+$ region. With this definition of regions we find that the HOMO and LUMO wave functions (see Figures 3 and 4) are found to have a weight in excess of 0.97 in the 3′G and $TOTA^+$ regions, respectively, with less than 0.02 in any other region.

(60) Moller, A.; Nordheim, A.; Kozloski, S. J.; Rich, A. *Biochemistry* **1984,** *23,* 56−62.

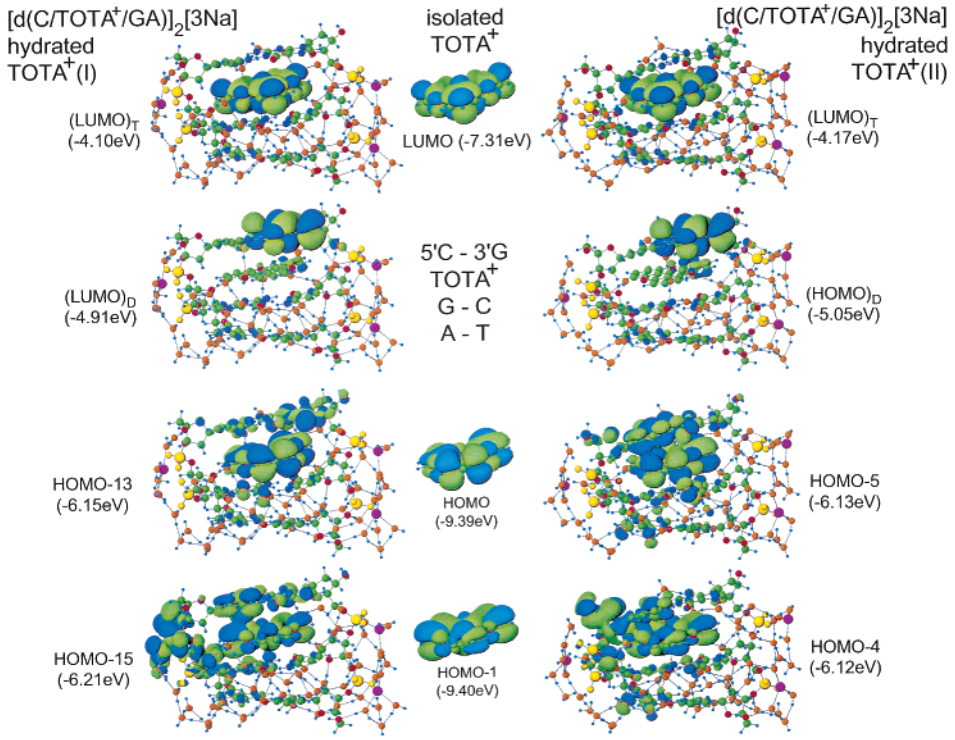

Figure 13. Orbital portraits for the isolated $TOTA^+$ (middle column), for the hydrated $TOTA^+$(I) 3-bp duplex DNA segments (left column), and for the $TOTA^+$(II) segment (right column). Orbital isosurfaces of different signs are distinguished by colors (blue and green), with the contours between the two colors describing the nodal surfaces. The orbital isosurfaces are superimposed on the atomic structures of the corresponding species. The identities of orbitals displayed in the figure are denoted next to each orbital portrait, along with the energy eigenvalue.

Figure 10, and the corresponding orbital portraits are displayed in the third and fourth rows of Figure 13. Interestingly the $(HOMO)_T - (LUMO)_T$ energy gap in the isolated $TOTA^+$ ($\Delta_T = 2.08$ eV) is close to the energy separation between the LUMO of the intercalation complex and states of the complex that have maximal overlap with the $(HOMO)_T$ and $(HOMO - 1)_T$ of the isolated $TOTA^+$; these energy separations (denoted by Δ_T'; see Figure 10) are $\Delta_T' = 2.15$ and 1.95 eV for the $TOTA^+$(I) (column iv) and $TOTA^+$(II) (column v) intercalation sites, respectively.

These observations pertaining to "spectral rigidity" of the intercalator, together with the aforementioned lack of appreciable electron transfer to $TOTA^+$, lead us to conclude that electrostatic forces and induced polarization of the electronic distribution underlie the intercalation and binding process of $TOTA^+$ into DNA. This is further supported by the polarization charge plots shown in Figure 14, where the polarization charge is calculated as the charge difference: $\delta\rho = \rho\{d(5'\text{-C/TOTA}^+\text{/GA-3}')\text{-}[3Na]\}_{hyd} - \rho\{d(5'\text{-C//GA-3}')[3Na]\}_{hyd} - \rho\{TOTA^+\}$, where the species in the first term is neutral, that in the second term is singly negatively charged, and the third is $TOTA^+$. The upper panel shows $\delta\rho$ for the entire intercalated three-base-pair DNA segment [$TOTA^+$(I)], the plot shown in the middle panel excludes the intercalator region [5], and in the plot shown in the bottom of the panel the charge differences in the regions of the intercalator and the hydrating shell are excluded. On the left side of the middle panel, we display the charge difference in the $TOTA^+$ region extracted from the complex, viewed from above the plane of the molecule. In these charge-difference portraits, magenta regions correspond to those where excess electronic charge is induced by the intercalation process, and yellow regions correspond to those where depletion of the electronic charge is found. The induced polarization charge on the inner surface of the "intercalation cavity" (defined by the 5′C-3′G and G-C base pairs surrounding the inserted $TOTA^+$ from above and from below, respectively) is −0.36e (obtained by integrating over the magenta region of the cavity). The integrated depletion in the adjacent (yellow) region is 0.25e (the total polarization charge, integrated for the entire system, vanishes).

The interaction of the $TOTA^+$ with the negatively charged hydrated duplex d(5′C//GA-3′)[3Na], as well as with the polarization charge discussed above, accounts for the near rigid shift of the $TOTA^+$ region in the electronic energy-level spectrum relative to the spectrum of the isolated $TOTA^+$. The effect of hydration is to lower the occupied levels of the DNA component of the spectrum, which opens the gap Δ_g between the $(HOMO)_D$ of the complex (localized on the 3′-G) and the $(LUMO)_T$ of the complex (localized on the intercalated $TOTA^+$). The water molecules have little effect on the $TOTA^+$ part of the spectrum because their affinity toward the $TOTA^+$ is relatively small compared with their binding affinity to the DNA bases.

Conclusions

The experimental and computational studies reported here present a clear picture of the photochemical, structural, and electronic consequences of the interaction of $TOTA^+$ with duplex DNA. Intercalation is a complex phenomenon that distorts the DNA structure and causes electronic energy level shifts.

Solution-phase experiments indicate that $TOTA^+$ binds to DNA with a preference for G-C base pairs and triplex structures. The X-ray crystallographic data show unambiguously that

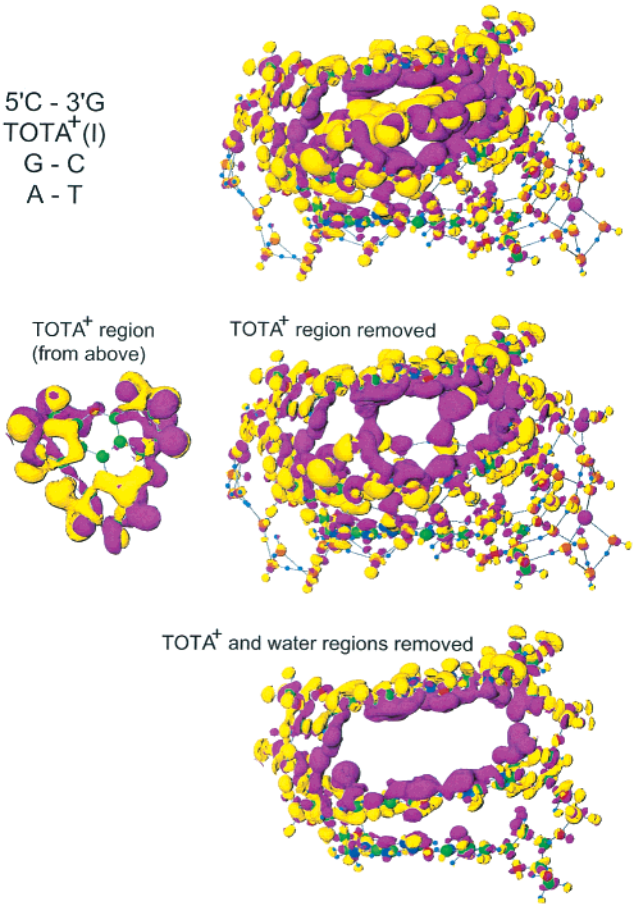

Figure 14. Polarization-charge ($\delta\rho$) isosurfaces (see text for details), calculated for the hydrated $TOTA^+$(I) 3-bp duplex DNA segments. Magenta regions correspond to those where excess electronic charge is induced by the intercalation process, and yellow regions denote those where depletion of charge ensued. The upper panel shows $\delta\rho$ for the entire hydrated $TOTA^+$-(I) 3-bp duplex segment; in the middle (right) panel, the $TOTA^+$ intercalator region is excluded; and in the bottom panel, both the $TOTA^+$ intercalator and hydration shell regions are excluded. The latter illustrates clearly the electronic polarization that is induced by the intercalation of the TOTA cation.

$TOTA^+$ intercalates into the DNA. Irradiation of the intercalated $TOTA^+$ with UV light results in a reaction at guanine that is revealed as strand cleavage, after treatment with piperidine, primarily at the 5′-G of a GG step. This pattern of reactivity has come to be associated with the one-electron oxidation of DNA to give a radical cation that is trapped at guanine by reaction with H_2O. $TOTA^+$ is a relatively inefficient sensitizer for this reaction, probably because it is reacting from an excited singlet state and back electron transfer competes successfully with migration of the radical cation.

The X-ray crystallographic data reveal that intercalation of $TOTA^+$ results in an unusually large extension of the helical rise of the DNA. This seems to be a result of unfavorable electronic interactions between $TOTA^+$ and the bases that form the intercalation site. The orientation of $TOTA^+$ is sensitive to hydrogen-bonding interactions with backbone atoms. In particular, intercavity hydrogen bonds provide stability and orientational specificity.

The electronic structure calculations reveal the importance of backbone, water, and counterions, which shift the energy levels of the DNA bases and the $TOTA^+$ orbitals significantly and differently. Importantly, the calculations show no meaningful charge transfer from DNA to $TOTA^+$ because $(LUMO)_T$ of $TOTA^+$ falls in the gap of $(HOMO)_D$ and $(LUMO)_D$. Consequently, the important electronic interactions are repulsive between occupied orbitals of $TOTA^+$ and occupied orbitals of the DNA bases. It is clear from the X-ray data and from the electronic calculations that electrostatic interactions control the intercalation of $TOTA^+$ in DNA. $TOTA^+$ strongly polarizes the intercalation cavity, where a sheet of excess electron density is induced that surrounds the $TOTA^+$.

Acknowledgment. We thank Professor W. David Wilson and Farial A. Tanious, of the Department of Chemistry, Georgia State University, for their assistance with the viscosity measurements and Dr. Jinsong Ren of the University of Mississippi Medical Center for her help with the competition dialysis assay. This work was supported by the National Science Foundation (G.B.S. and L.D.W.), by the National Cancer Institute (J.B.C.), and by Grant FG05-86ER-45234, U.S. Department of Energy (U.L.), for which we are grateful. Calculations were performed at Georgia Institute of Technology Center for Computational Material Science and at the National Energy Research Scientific Supercomputing Center (NERSC) at Lawrence Berkeley, California.

Supporting Information Available: Two tables listing crystallographic and refinement statistics for $d[CGATCG]_2 \cdot TOTA^+_2$ and base-step distances and overall DNA length of intercalated hexamers, diagram and calculation of partial charges on the TOTA cation, and preparation of hydrated samples for calculation (PDF). This information is available free of charge via the Internet at http://pubs.acs.org.

JA0211196